


## Article

# Prediction of Clearance Vibration for Intelligent Vehicles Motion Control

Yunhe Zhang<sup>1</sup>, Faping Zhang<sup>1,\*</sup> , Wuhong Wang<sup>1</sup>, Fanjun Meng<sup>2</sup>, Dashun Zhang<sup>3</sup> and Haixun Wang<sup>3</sup>

<sup>1</sup> School of Mechanical Engineering, Beijing Institute of Technology, Beijing 100081, China; he005@126.com (Y.Z.); wangwuhong@bit.edu.cn (W.W.)

<sup>2</sup> School of Mechanical and Electrical Engineering, Changchun University of Science and Technology, Changchun 130013, China; mengfanjun168168@126.com

<sup>3</sup> The 55 Research Institute of China North Industries Group Corporation Limited, Changchun 130012, China; zhangdashun666@126.com (D.Z.); 13756675662@126.com (H.W.)

\* Correspondence: zhangfaping@bit.edu.cn; Tel.: +86-010-6891-2708

**Abstract:** Motion control analysis should consider the system's uncertainty to ensure the intelligent vehicle's autonomy. The clearance structure of the transmission shaft is modeled as a cantilever beam with double clearance to predict the clearance vibration for mitigating the nonlinearity. Based on the Kelvin–Voigt collision model, a clearance model was developed using time-varying parameters identified by the wavelet transform. Comparing the frequency response functions (FRF) of the initial model with constant parameters and the updated model with time-varying parameters, the experimental results from the updated model indicate that the modal assurance criterion (MAC) is increased by 42.92%, 31.08%, 38.97%, and 50.74% in the first-four order. Cross-signature assurance criteria (CSAC) and cross-signature scale factor (CSF) have been increased by 6.55% and 12.37%. The control method based on the clearance model has been verified. In the case of 120 km/h, compared with model-predictive control (MPC) and sliding mode control (SMC), the peak of the lateral position error was reduced by 35.7% and 14.3%, and the peak of the heading error was reduced by 50% and 15.6%.

**Keywords:** intelligent vehicle; motion control; clearance nonlinearity; parameter identification; frequency response function



**Citation:** Zhang, Y.; Zhang, F.; Wang, W.; Meng, F.; Zhang, D.; Wang, H.

Prediction of Clearance Vibration for Intelligent Vehicles Motion Control. *Sustainability* **2022**, *14*, 6698.

<https://doi.org/10.3390/su14116698>

Academic Editors: Xiaoyuan Wang, Junyan Han and Gang Wang

Received: 20 April 2022

Accepted: 27 May 2022

Published: 30 May 2022

**Publisher's Note:** MDPI stays neutral with regard to jurisdictional claims in published maps and institutional affiliations.



**Copyright:** © 2022 by the authors. Licensee MDPI, Basel, Switzerland. This article is an open access article distributed under the terms and conditions of the Creative Commons Attribution (CC BY) license (<https://creativecommons.org/licenses/by/4.0/>).

## 1. Introduction

Intelligent vehicles provide an alternative solution to the growing problems of pollution, traffic accidents, and energy shortages [1]. Motion control is key to achieving autonomous movement. Based on the information provided by sensors, the intelligent vehicle is controlled in real time to follow the desired trajectory [2]. The control methods include adaptive control, robust control, and intelligent control.

For adaptive control, Colbaugh et al. combined adaptive control and homogeneous system theory to address the motion control for uncertain mobile manipulators [3]. Huang et al. were able to control the motion of wheeled mobile robots by adaptive control. Compared to a model-free PID controller, the tracking effect of track was faster and more accurate [4]. Tasi designed a new adaptive controller to provide progressive stabilization of intelligent parking spaces [5]. Fukao, Dixon, and Tayebi et al. developed a controller for tracing uncertain mobile robots using the backstepping method [6–8]. Sun provided the vehicle attitude control system with a fuzzy PID. Based on the fuzzy relationship between three PID control parameters and deviation signals, the online PID control parameters were adjusted to reduce the deviation of the vehicle attitude control system. As a result, the random interference and uncertainty of vehicle motion were reduced [9]. For the ASV and the sway, surge, and yaw directions, Maajid used three parallel fuzzy adaptive PID controllers [10]. In order to overcome the high uncertainties in acceleration and braking, Wei

proposed an adaptive sliding mode control method based on feedback linearization [11]. To ensure that the vehicle follows the trajectory created by the driver, Temiz proposed a parameter integration fault-tolerant vehicle monitoring algorithm based on online updates [12]. In the process, adaptive control is suitable for solving nonlinear, time-varying, and hysteretic problems due to its high robustness. However, adaptive control fails to provide a general solution. Control accuracy and parameter estimation are inconsistent in some controllers. They do not meet the requirements for dynamic performance during the startup and transition process.

For robust control, Lucibello et al. designed robust stabilization controllers for nonlinear chains to ensure robustness [13]. In order to achieve precise path tracking of a two-degree-of-freedom mobile robot (WMR), Chung et al. developed a double loop (speed loop and position loop) path tracking controller based on robust control methods [14]. In order to track wheeled robots with bounded errors in the position feedback information, Hamel et al. developed a robust tracking controller [15]. Lee used the switching controller method to stabilize nonholonomic chain systems, ensuring the system's robustness and fast convergence of errors [16]. Jia investigated the robust control of four-wheel-drive vehicles with uncertain velocity, moment of inertia, mass, and friction coefficient. Based on the established vehicle dynamics model, a robust control scheme was developed to limit the influence of changes in vehicle parameters on steering performance [17]. To improve the lateral stability of tractors and semitrailers, Liu proposed a robust H $\infty$ optimal control scheme [18]. Li proposed a method to improve lateral vehicle stability using output feedback control [19]. Robust control systems are particularly effective for ensuring stability and reliability as the primary objectives. The dynamic process characteristics can be predicted without establishing a formal process model. Therefore, robust control is particularly suitable for systems with large uncertainty ranges and small stability margins. However, due to the robust control system generally failing to operate in the optimal state, steady-state accuracy is relatively low.

For intelligent control, Chen proposed the RBF neural network sliding mode control method to improve control accuracy and robustness due to many external disturbances during driving [20]. Chang proposed controlling trajectories to enhance efficiency and accuracy by a neural network [21]. Jia developed a robust adaptive control algorithm using RBF neural networks and improved the fractional integral sliding mode control. In complex underwater conditions, accuracy and stability were enhanced in the underwater docking process for autonomous underwater vehicles (AUVs) [22]. Henaff et al. developed an intelligent vehicle controller based on neural networks [23]. In a dynamic model of the inverted pendulum system, Kim compensated for parameter uncertainty errors using a neural network control strategy [24]. Rusu and Wang et al. combined neural network control and backstepping to create a tracking controller for mobile robots [25,26]. By combining neural network and backstepping control methods, Fierro et al. developed a tracking controller for the intelligent vehicle to ensure asymptotic stability [27]. Choomuang developed an obstacle avoidance/tracking controller for the intelligent vehicle using the Kalman filter and fuzzy control method [28]. Because intelligent vehicles operate in complex environments containing unpredictable disturbances, the traditional dynamic model based on precise motion control was no longer appropriate. Butcher and Eli developed a fuzzy control system to ensure accurate tracking and robustness [29,30]. Intelligent control enables systems to run efficiently, solve generalized problems, and offer fault tolerance.

Moreover, it is capable of compensating and judging. Intelligent control does not clearly distinguish between controller and object. Compared with the traditional automatic control, the intelligent control objects have substantial uncertainty. The intelligent control is also limited to the particular requirements and conditions of the algorithm.

Furthermore, a sliding mode control method is also an exhaustive control algorithm. Due to its ability to overcome the system uncertainty, sliding mode control exhibits strong robustness to interference and unmodeled dynamics in the nonlinear control systems [31].

The clearance of the transmission shaft is introduced into the control method to improve the accuracy and stability further.

However, the system nonlinearity is usually ignored in motion control or merely mitigated through simple error compensation. The previous study focused on the uncertainty in motion control based on simplifying the dynamics model. However, the simplified model cannot reflect the actual situation when the speed is high, and the mass is large. Intelligent vehicles are complex systems with multiple inputs and outputs, strong coupling, and significant nonlinearities. The mass, inertia, and tire friction coefficient parameters have measurement noise and uncertainty.

Additionally, the actuator exhibits nonlinearity (clearance, friction, and dead zone). Due to the clearance nonlinearity, the control precision is limited by the qualitative analysis, not quantitative analysis. Thus, it is imperative to analyze the quantitative analysis of clearance nonlinearity to eliminate the influence and effectively track the trajectory.

For clearance analysis, Tian developed various dynamic models to describe the dynamic clearance characteristics, establishing a theoretical basis for the subsequent research on clearance dynamics [32]. Using the clearance model abstracted into the spring-damping model, Liu constructed a dynamic cantilever beam model with double clearance. Dynamic information determines the clearance value to control the nonlinear clearance error within a reasonable range [33]. Yang carried out an experimental and numerical analysis for the free vibration modes of the clearance cantilever beam, derived the mathematical expression of the simplified clearance stiffness, and verified the calculated frequency with the experimental data. It was found that the measured frequency was in good agreement with the predicted frequency [34]. To study the dynamic behavior of planar mechanical systems with joint clearance, Bai and Zhao developed a hybrid contact force model in conjunction with Lankarani–Nikravesh and Winkler elastic foundation models [35]. Khantiwada proposed a relationship between force and deformation based on the Hunt–Crossley collision model and accurately calculated damping constants. Comparisons of linear and nonlinear Hunt–Crossley models with other models were performed to verify the model validity [36]. A rotary joint model with radial and axial clearances was developed by Marques [37].

The desired trajectory was tracked by controlling the transmission mechanism under a control algorithm, taking the clearance factor into account. Control precision affects the safety and stability of intelligent vehicles. The vehicle's speed is usually set to a constant value subjectively in intelligent vehicle lateral control research on narrow curved roads. The control strategy can track the desired trajectory accurately. However, the transmission system accuracy may influence the vehicle tracking control with the preview system for roads with large curves. With high speed and large curvatures, a small transmission error can adversely affect the performance and stability of the intelligent vehicle tracking control. Furthermore, the speed is set subjectively as the expected speed lacks the ability to adapt to the vehicle in real time. As a result, the vehicle's state cannot be accurately adapted for velocity changes in real time, resulting in sideslip or even roll-over, which directly impacts the vehicle's control effect and local stability. In order to improve the motion control performance of an intelligent vehicle, the nonlinearity influence is estimated by predicting the clearance vibration. Stability and rapidity are improved to meet the driving requirements. This paper uses the time-varying parameters to describe clearance dynamics in contact moments.

The paper is organized into three sections. First, a dynamic clearance model is presented based on the Hamilton principle and the modal hypothesis. The hysteresis model is introduced to describe the lubrication impact on clearance further. Second, the wavelet transform determines the time-varying stiffness and damping. Finally, the effectiveness of the modeling method is verified by establishing an experimental model and comparing the relevant error indicators of the FRF. The clearance model is introduced into the sliding mode control, and a control method considering the gap nonlinearity is proposed, verified by simulation. Finally, the effectiveness of the modeling method is examined by establishing

an experimental model and comparing the relevant error indicators. A control method based on clearance nonlinearity is proposed and validated by simulation.

### 2. Nonlinear Modeling for Clearance

The intelligent vehicle actuator consists of a connecting rod transmission mechanism, and the output shaft is connected to the front wheel to control the wheel deflection. A typical nonlinearity in the transfer system is the shaft clearance. In the transmission link of the servo system, the nonlinear position error is caused by the clearance. As a result, the dynamic performance and steady-state accuracy are negatively affected. In contact collision between the axis and bearing for a long time, clearance value will also increase, aggravating the nonlinear vibration of the transmission shaft. At the same time, the change in clearance size also impacts the control precision.

As the demand for high-precision control systems increases, more research is being conducted on clearance nonlinearity. Because of clearance in multiple systems, damping and stiffness exhibit different nonlinearities. Transmission system clearances directly impact the error compensation strategy and the control precision.

Therefore, the paper analyzes vibration generated by driveshaft clearance to improve the vibration prediction accuracy and ensure precise error compensation. The shaft is abstracted as a cantilever beam based on the dynamic characteristics. As illustrated in Figure 1, based on the clearance model [38], the bearing bush lengths and the grease hysteresis in clearance are introduced to construct a cantilever beam with double clearance. The left end of the beam is fixed, while the right end can be moved.

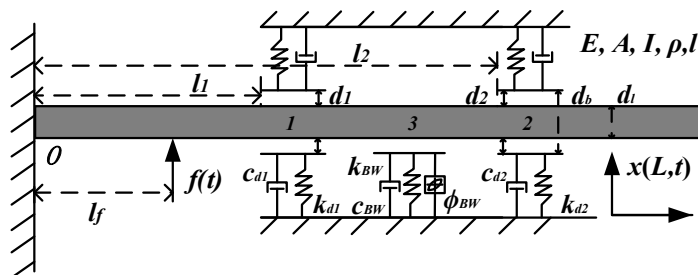


Figure 1. Simplified model of cantilever beam with double clearance.

In Figure 1,  $l_1, l_2, l_f$  represent the distance between the fixed end  $O$  to the clearance 1, clearance 2, and the excitation.  $E, A, I, \rho, l$  are Young’s modulus, cross-sectional area, moment of inertia, density, and length of the cantilever beam. The clearance values:  $d = d_1 = d_2 = (d_1 - d_b)/2$ .  $d_b$  and  $d_i$  are the outer diameter of the beam and the inner diameter of the bearing bush.  $k_{d1}, k_{d2}$  and  $c_{d1}, c_{d2}$  are stiffness and damping at clearance 1 and 2.  $x(L, t)$  is the vertical displacement,

$$x(L, t) = \sum_1^n Y_i(L)p_i(t) \tag{1}$$

$Y_i(x), p_i(t), i$  are modal shape function, coordinates, and the mode order. The boundary conditions of the cantilever beam are

$$\frac{\partial^2 x(L, t)}{\partial L^2} \Big|_{L=0} = 0; \quad \frac{\partial^3 x(L, t)}{\partial L^3} \Big|_{L=0} = 0; \quad \frac{\partial^2 x(L, t)}{\partial L^2} \Big|_{L=l} = 0; \quad \frac{\partial^3 x(L, t)}{\partial L^3} \Big|_{L=l} = 0 \tag{2}$$

Based on the Hamilton principle and assumed modal method, a dynamic model of the cantilever beam with double clearance is established:

$$M_{pi}\ddot{p}_i + C_{pi}\dot{p}_i + K_{pi}p_i + Y_i(l_1)f_1(t) + Y_i(l_2)f_2(t) + V_i(l_3)\phi_{BW}(t) = Y_i(l_f)f(t) \tag{3}$$

$M_{pi}$ ,  $K_{pi}$ ,  $C_{pi}$  represent the  $i$ -order modal mass, stiffness, and damping.  $f_{d1}(t)$ ,  $f_{d2}(t)$ ,  $f(t)$  represent the nonlinear forces at positions 1, 2,  $l_f$ . The following formula can calculate each parameter:

$$M_{pi} = \int_0^l \rho A Y_i^2 dx \quad (4)$$

$$K_{pi} = \int_0^l EI (Y_i'')^2 dx = \int_0^l Y_i EI (Y_i')'' dx \quad (5)$$

$$C_{pi} = \eta_1 M_{pi} + \eta_2 K_{pi} \quad (6)$$

$$Y_i(x) = \cos \beta_i x - ch \beta_i x + \frac{\sin \lambda_i - sh \lambda_i}{\cos \lambda_i - ch \lambda_i} (\sin \beta_i x - sh \beta_i x) \quad (7)$$

$\eta_1$  and  $\eta_2$  represent Rayleigh damping parameters.  $\beta_i$  is the order of frequency equation. The characteristic roots  $\lambda_i$  of the frequency equation satisfy Equation (8), and  $\lambda_i = (2i + 1)\pi/2$ .

$$\cos \lambda_i ch \lambda_i = 1 \quad (8)$$

The hysteresis model is composed of a linear spring-damper  $k_{BW} - c_{bw}$  and a nonlinear B-W element. The B-W element provides the hysteresis force by the Coulomb friction block. The mechanical model has two degrees of freedom: particle displacement and hysteresis displacement [39]. The dynamic equation is expressed as follows:

$$\begin{cases} \phi_{BW}(x, \dot{x}) = \lambda kx + (1 - \lambda)kx_{BW} \\ \dot{x}_{BW} = A\dot{x} - \zeta|\dot{x}||x_{BW}|^{n_{BW}-1}x_{BW} - \gamma\dot{x}|x_{BW}|^{n_{BW}} \end{cases} \quad (9)$$

The restoring force is constituted by linear force  $\lambda kx$  and hysteresis force  $(1 - \lambda)kx_{BW}$ .  $\lambda$  determines the weight of the nonlinear and linear.  $A$ ,  $\zeta$ ,  $\gamma$  control the shape of the hysteresis loop. The order is usually 2.

Based on the nonlinear clearance force  $f_d(t)$  and the damping loss in the collision process, the Kelvin–Voigt model (a set of parallel linear spring-damping units) is adopted to describe the collision characteristics [40], expressed as follows:

$$f_d(t) = c_d(t)\dot{g}(t) + k_d g(t) \quad (10)$$

$g(t)$  are the displacement and velocity functions at the clearance position. The expression is as follows:

$$g(t) = \begin{cases} x(l, t) - d & x(l, t) \geq d \\ 0 & -d < x(l, t) < d \\ x(l, t) + d & x(l, t) \leq -d \end{cases} \quad (11)$$

A dynamic model of the double-clearance cantilever beam was developed to describe the dynamic characteristics of the drive shaft. The grease facilitated a smooth movement during collisions and recovery at the clearance. The grease forms change with collision, resulting in a complex interactive relationship. However, the constant damping in the Kelvin–Voigt model cannot accurately replicate the actual vibration laws. In order to overcome the limitations of the Kelvin–Voigt model, a spring-damping model using time-varying parameters is developed to model the dynamic process. Energy loss is nonlinear and time-varying at the re-contact moment after passing the contact point.

The time-varying parameters of the collision model are identified using wavelet transform theory. The validity of the identification algorithm is examined in the following section.

### 3. Parameter Identification Based on Wavelet Transform

This section aims to establish a time-varying parameters clearance model that can accurately predict the vibration caused by the clearance. The instantaneous damping ratio and frequency are calculated with wavelet ridges and skeletons. Due to the nonlinear-

ity of clearance and lubrication, it is impossible to identify the contact force using the same scale accurately. Wavelet analysis can provide a variable time-frequency window to obtain more local information in some methods for parameter identification. Based on the analysis of high-frequency signals, the adaptive window size narrows automatically and grows wider for low-frequency signals [41]. For non-stationary response signals of the output system, time-frequency analysis provides an effective method for identifying time-varying parameters.

### 3.1. Time-Varying Parameter of Clearance Structures

The test signal is assumed to be  $g(t)$  at a certain point of the cantilever beam with double clearance under excitation. The wavelet transform is  $W(a, b)$ . The ridges of the wavelet transform  $(a, b)$  represent a series of points. A wavelet ridge's envelope coefficient is defined as the skeleton. A wavelet ridge and skeleton model can estimate the system's natural frequency and damping ratio [42].

For the response signal of the cantilever beam system:  $x(t) = e^{-\zeta(t)\omega t} \cos(\omega t + \varphi)$ , the instantaneous damping ratio is

$$\zeta = -\frac{d[\ln(A(t))]}{\omega dt} \quad (12)$$

In combination with the wavelet center frequency  $\omega_0$ , scale factor  $a$ , translation factor  $b$ , wavelet coefficient  $W(a, b)$ , and instantaneous amplitude  $A(t)$ , the instantaneous frequency  $\omega$  is represented as follows:

$$\omega = \frac{\omega_0}{a}; A(t) = \frac{2[W(a, b)]}{\sqrt{a}} \quad (13)$$

Assuming that the mass is constant and known, the time-varying stiffness obtained by the identification system is

$$k(t) = m\omega^2 \quad (14)$$

As a result of the internal friction of solid materials and the effects of decoupling, the clearance vibration can be represented by the classical Rayleigh damping model and the complex damping model [43,44]. The dynamics model may be decoupled while maintaining the modal information. It can be written as

$$c(t) = \alpha_0 m + \alpha_1 k(t) + \alpha_3 j k(t) \quad (15)$$

$m$  and  $k(t)$  represent the equivalent mass and time-varying stiffness of the cantilever beam at the clearance position. Furthermore, the coefficients of the Rayleigh damping model and complex damping model are expressed as

$$\begin{aligned} \alpha_0 &= 2\omega\zeta \\ \alpha_1 &= 2\zeta/\omega \\ \alpha_3 &= 2\zeta \end{aligned} \quad (16)$$

As a consequence, the nonlinear damping model is expressed as follows:

$$c(t) = 4m\omega\zeta(t) + 2\zeta j m \omega^2 \quad (17)$$

The instantaneous frequency and damping ratio are estimated by analyzing the wavelet ridge and skeleton using the variable time-frequency window. Clearance models are built with time-varying stiffness and damping. Next, the wavelet transform algorithm is demonstrated numerically.

### 3.2. Parameter Identification and Verification

This section uses step and continuous function parameter models to verify identification accuracy. In order to analyze the performance of the identification algorithm against noise, SNR of 20 dB and 100 dB are applied. Other mechanical parameters did not change over time.

$$\text{Working condition 1: Step function value: } c(t) = \begin{cases} 0.02, & (t < 2) \\ 0.04, & (t \geq 2) \end{cases}, k(t) = \begin{cases} 8000, & (t < 2) \\ 5000, & (t \geq 2) \end{cases}.$$

Working condition 2: Continuous function value:  $c(t) = 0.02 - 0.02t$ ,  $k(t) = 8000 - 1000t$ .

The wavelet transform is used to identify the damping and stiffness. In Figures 2 and 3, damping and stiffness identification results for SNR = 20 and SNR = 100 are presented. For SNR = 100, the identified and theoretical values were kept within a low error range. Compared to SNR = 100, the relative error between the identified and theoretical values is greater with SNR = 20. In this case, it can be seen from the comparison that the identification effect of damping parameters is well within the stable range. However, in abrupt changes, the identification effect will fluctuate. As a whole, the identification result is tracked accurately, and it fluctuates around the theoretical value. Therefore, the method can accurately identify the theoretical value change at the mutation moment.

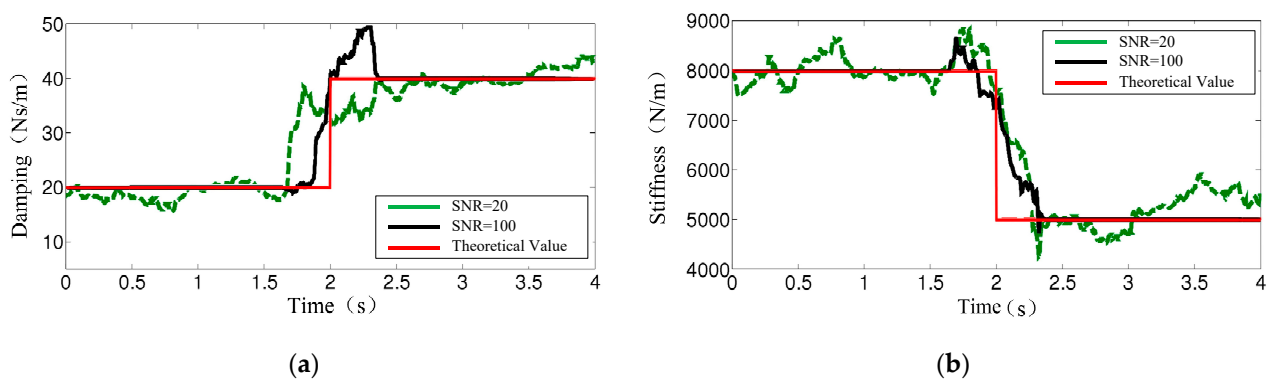


**Figure 2.** Identification results: (a) is step damping identification results; (b) is step stiffness identification results.

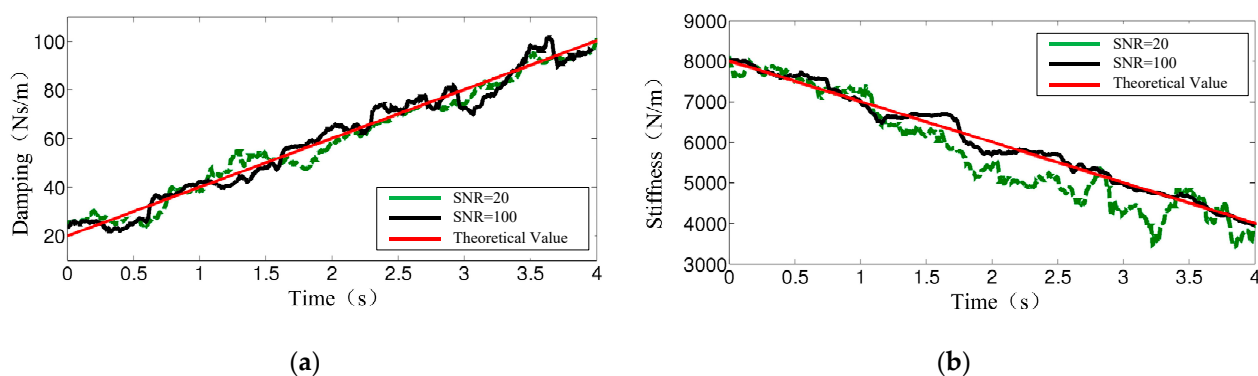


**Figure 3.** Identification results: (a) is continuous damping identification results; (b) is continuous stiffness identification results.

The effectiveness of the identification method has been demonstrated in numerous cases. Noise and scale factors affect the identification accuracy. According to Formula (13), the scale factor is a significant determinant of identification accuracy, influencing the relationship between accuracy and efficiency. The scale factor reduces as the translation factor increases. As part of maintaining an exact similarity, the scale factor is used to

“extend” or “compress” the wavelet. It is necessary to select the scale parameter precisely to improve the time-varying parameter model.

In order to reduce the error and improve the identification accuracy, it is necessary to analyze the design parameters in the identification process. In the case of the continuous damping function:  $c(t) = 0.06 - 0.0002t$ , multi-scale identification is conducted to compare and analyze the identification results over a range of scales. The selection and dispersion of scale factors in the recognition process is described in computational efficiency and parameter recognition accuracy.

Setting the range  $[2^{-5}, 2^{-8}]$  has three discrete scale sequences. Translation parameters:  $b = a(16k + x8)$ ; variable parameters:  $k = 0 : 0.005 : T/(4a)$ .

1.  $a = 2^{-5}, 2^{-6}, 2^{-7}, 2^{-8}$ ;
2.  $a = 2^{-6}, 2^{-6.25}, 2^{-6.5}, 2^{-6.75}, 2^{-7}$ ;
3.  $a = 2^{-6.5}, 2^{-6.6}, 2^{-6.7}, 2^{-6.8}, 2^{-6.9}, 2^{-7}$ .

Based on the method proposed in this section, three different analytical scale sequences are used, as shown in Figure 4. The solid line represents the theoretical value, and the dotted line represents the identification result at different scales.

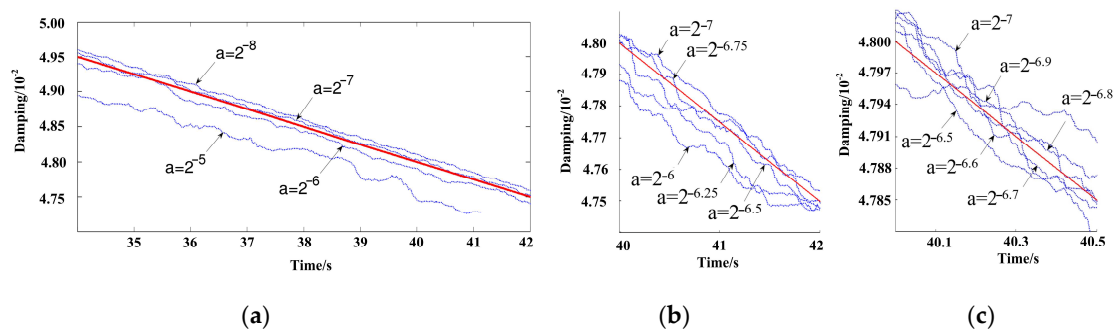


**Figure 4.** Parameter identification based on different sequences: (a–c) represent the comparison of identification results at scales 1, 2, and 3, respectively.

In sequence 1, identification results were the worst with  $a = 2^{-5}$ . The discrimination accuracy is improved obviously with  $a = 2^{-6}$  and  $a = 2^{-7}$ . However, the identification results are dramatically reduced with  $a = 2^{-8}$ . Therefore, the analysis scale should be selected between  $a = 2^{-6}$  and  $a = 2^{-7}$ . In sequence 2, the accuracy of identification results is better than other scales with  $a = 2^{-6.5}$ ,  $a = 2^{-6.5}$ ,  $a = 2^{-7}$ . However, as the scale factor value becomes smaller, the calculation amount increases. The number of corresponding translation parameters is 3200, 3800, 4400, 5200, and 6400 in five factors. In the smaller scale interval of sequence 3, the dispersion is more intensive. The identification result is the best at  $a = 2^{-6.8}$ , but the amount of calculation and analysis increases significantly.

The smaller the analysis scale between the discrete scales of the three sequences, the more intensive the corresponding translation parameters. However, the more accurate the analysis, the more computational time and resources are required. In addition, estimating the scale factor affects identification accuracy and calculation efficiency. The wide intervals and long discrete methods should be selected based on the above analysis.

Based on the identified time-varying stiffness and damping, a time-varying parameter clearance model is derived to describe the vibration caused by clearance. The credibility of the identification algorithm is verified in the case of continuous and step functions. An experimental model based on time-varying parameters is used to determine the validity of the cantilever beam with double clearance.

#### 4. Results and Discussion

In order to accurately predict the transmission shaft vibration caused by the clearance, the transmission shaft is abstracted as a cantilever beam with double clearance. A dynamic



model of the cantilever beam double clearance has been developed using the wavelet transform to identify time-varying parameters in clearance. Next, the accuracy of vibration prediction is demonstrated by constructing a test platform.

#### 4.1. Test Model

Figure 5 shows the structure model, while Figure 6 shows the test model. Sensors 1–8 are installed on the beam. A Fisher information criterion is used to optimize the arrangement [45]. Shakers applied random loads to the bottom plate, and sensors measured the dynamic response of each position. The signal is processed by the data acquisition system and transmitted by the power amplifier to the computer.

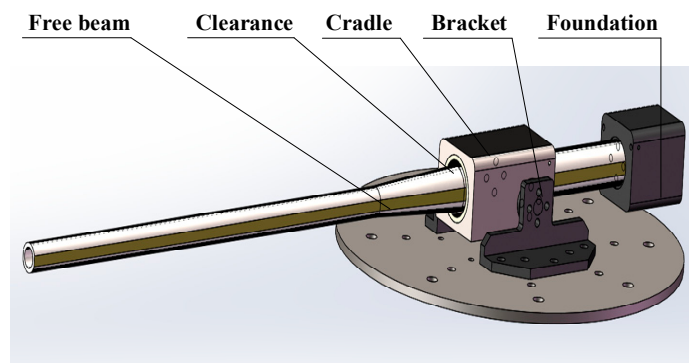


Figure 5. Structure model.

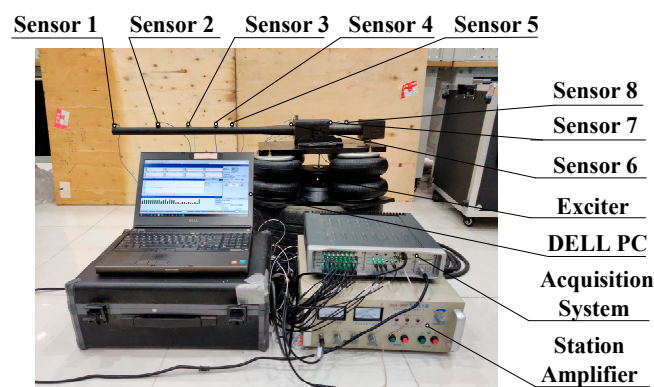


Figure 6. Test model.

#### 4.2. Validity of Clearance Model

FRF is calculated by testing the measured position. In Figure 7, the FRF comparison is performed for the clearance positions (sensors 6 and 7). The blue, black, and red lines indicate the initial model based on constant values, the updated model based on parameter identification, and the test model. Initial and updated models agree well with experimental results at first-order and second-order frequencies. FRF error increases significantly between the initial and test models at third-order and fourth-order frequencies. By comparing the amplitude of FRF, the updated model is closer to the test model.

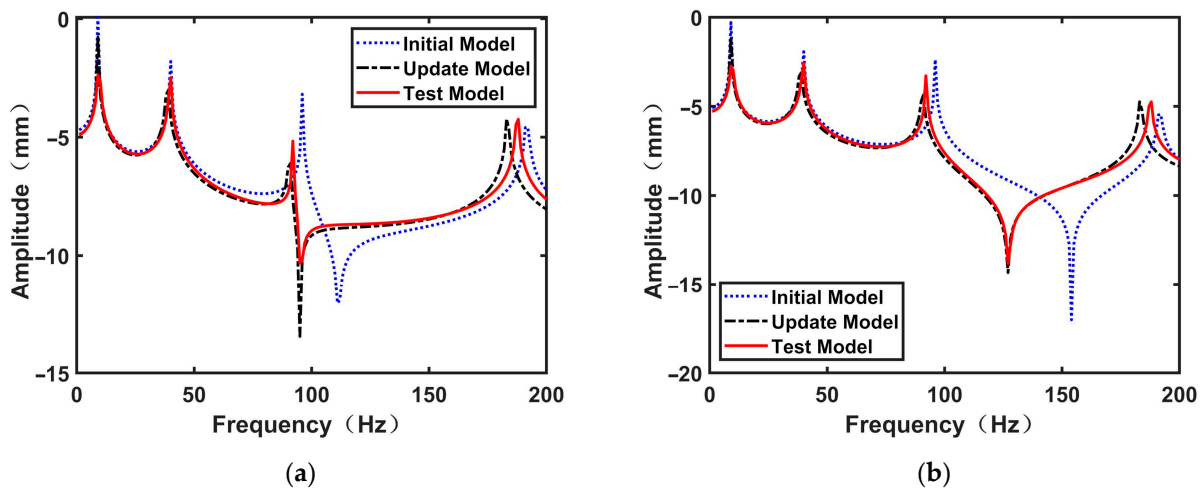


Figure 7. FRF of clearance position 1 and 2: (a) is position 1 for sensor 6; (b) is position 2 for sensor 7.

Figure 8 illustrates the comparison of FRF at the measurement points 1, 2, 3, 4, 5, and 8. First-order and second-order models may better reflect the test model with the initial and updated models. However, the difference between the initial and test models increases after the second order. In contrast, the updated model can reflect the changes in the FRF of the test model. Nevertheless, the updated model will contain some errors at the fourth-order position. The noise increased with identification times, which led to reduced accuracy. However, the updated model can better reflect the dynamic characteristics of the test model.

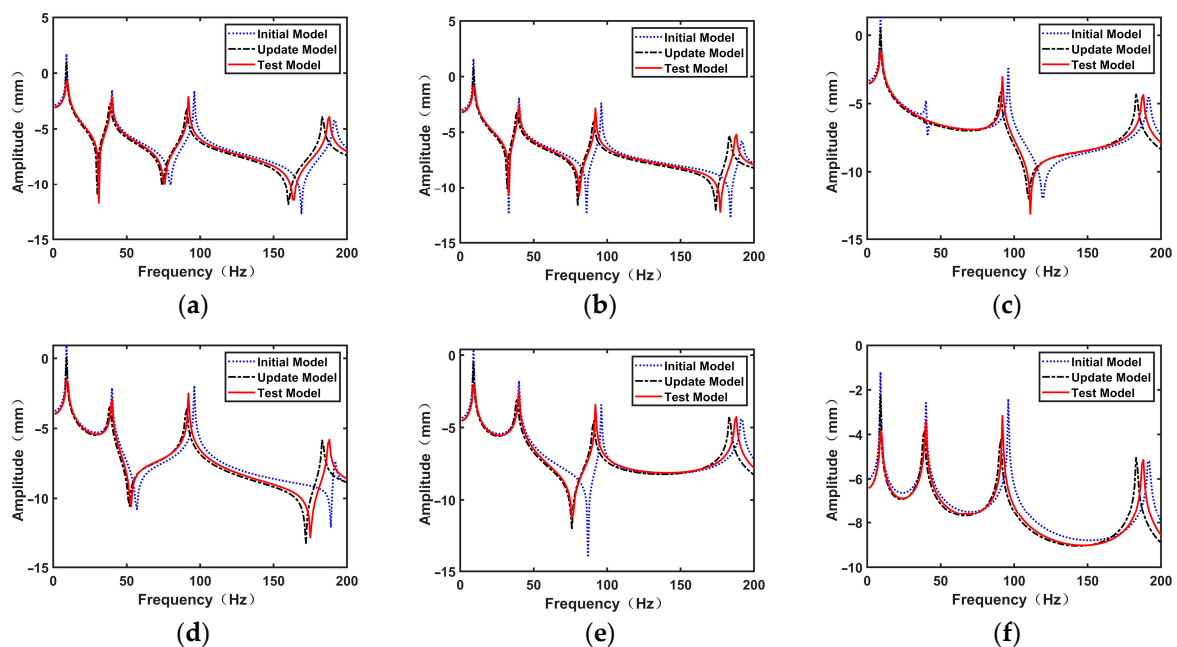


Figure 8. FRF of other position: (a–f) represent the comparison of FRF at sensor measuring points 1, 2, 3, 4, 5, 8.

A correlation analysis is performed using relative error and MAC to examine the differences between the initial and updated models in natural frequencies, as shown in Table 1. Compared to the original model, relative errors of the updated model are

reduced by 0.54%, 2.26%, 4.09%, and 0.47%. The MAC grows by 42.923%, 31.083%, 38.97%, and 50.743%.

**Table 1.** Comparison of natural frequency errors.

Order	Frequency (Hz)	Initial Model Based on Constant Damping			Updated Model Based on Time-Varying Damping		
		Frequency (Hz)	RE (%)	MAC	Frequency (Hz)	RE (%)	MAC
1	9.25	9.15	1.0811	0.5378	9.2	0.5405	0.9422
2	39.75	38.35	3.5220	0.6283	40.25	1.2579	0.9117
3	92.85	97.85	5.3850	0.5265	91.65	1.2924	0.8627
4	188.85	191.35	1.3238	0.4183	187.25	0.8472	0.8492

In addition to comparing errors at natural frequencies, the error at other frequencies may also reflect the correlation degree between the models. Next, the MRE, RMSE, FRAC, CSAC, and CSF are examined as evaluation indicators. CSF and CSAC indicate the FRF correlation degree between the numerical and test models at each frequency. This value ranges from 0 to 1, for which a value closer to 1 indicates greater accuracy [46]. The comparison is presented in Table 2.

**Table 2.** FRF errors in measuring points.

Position	Initial Model Based on Constant Damping					Updated Model Based on Time-Varying Damping				
	MRE	RMSE	FRAC	CSAC	CSF	MRE	RMSE	FRAC	CSAC	CSF
1	0.8013	1.4181	0.8643	0.8891	0.8410	0.5763	0.7481	0.9443	0.9633	0.9619
2	0.8078	1.3410	0.7708	0.8921	0.8485	0.5827	0.5902	0.9507	0.9531	0.9608
3	0.7963	1.5589	0.8593	0.8847	0.8363	0.5785	0.6026	0.9465	0.9677	0.9656
4	0.8050	1.3795	0.8680	0.8812	0.8459	0.5810	0.5946	0.9490	0.9487	0.9652
5	0.7970	1.6391	0.6600	0.8973	0.8431	0.5799	0.6574	0.9479	0.9375	0.9599
6	0.7938	1.9037	0.8568	0.8956	0.8392	0.5777	0.0976	0.9457	0.9567	0.9568
7	0.8007	1.0062	0.6373	0.8870	0.8371	0.5778	0.2419	0.9458	0.9532	0.9521
8	0.7969	1.3674	0.8599	0.8912	0.8457	0.5743	0.7174	0.9423	0.9372	0.9657
Means	0.7999	1.4517	0.7971	0.8898	0.8421	0.5785	0.5312	0.9465	0.9522	0.9610

Following the comparison, the relative error and RMSE are reduced by 27.67% and 63.41% for the updated model based on parameter identification. The FRAC has improved by 15.79%, while the value exceeds 94%. As shown in Figures 9 and 10, CSAC and CSF have increased by 6.65% and 12.37%, over 90%. In the updated model, the CSAC and CSF have increased significantly at natural frequencies close to one. It is confirmed that the updated model can reflect the frequency domain characteristics of the test model.

In this section, experimental verification is carried out using the established experimental platform. In comparing the FRF of the initial and updated model, the model was evaluated by the relative error and MAC to prove the validity of the updated model. In addition, by comparing the MRE, RMSE, FRAC, CSAC, and CSF, the updated model would well reflect the dynamic characteristics of the test model.

Experimental verification is carried out in this section using the established experimental platform. Using the FRF of the initial and updated model, the model was evaluated by the relative error and MAC to determine the validity of the updated model. Furthermore, MRE, RMSE, FRAC, CSAC, and CSF are compared. The updated model would reflect the dynamic characteristics of the test model.

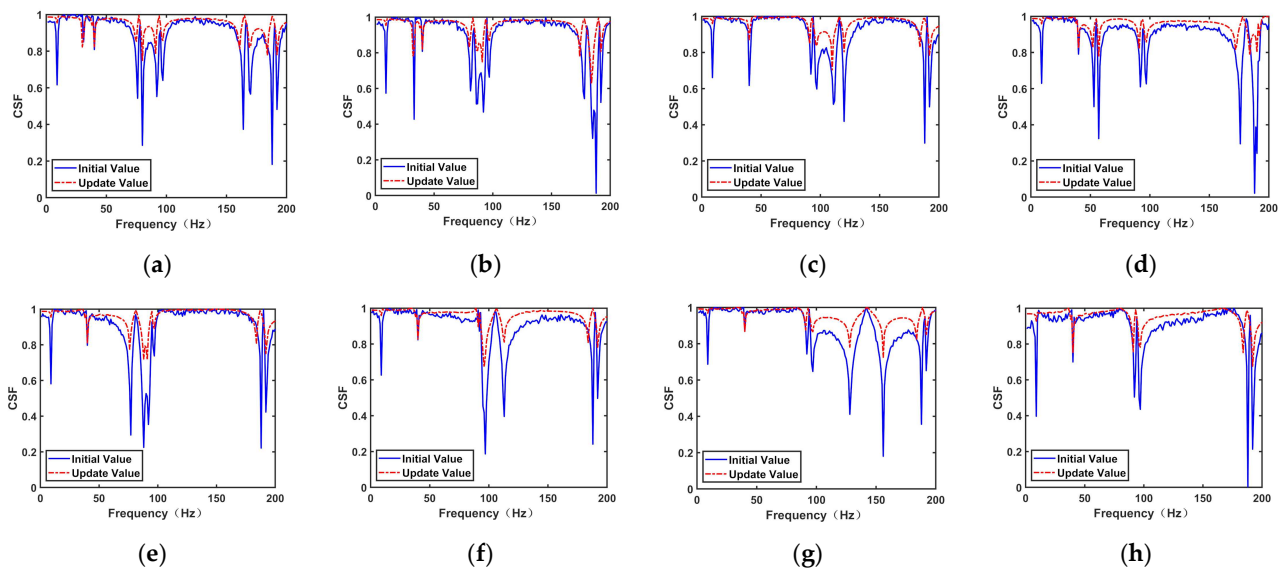


**Figure 9.** Comparison of CSAC: (a–h) represent the comparison of CSAC at sensor measuring points 1, 2, 3, 4, 5, 6, 7, 8.

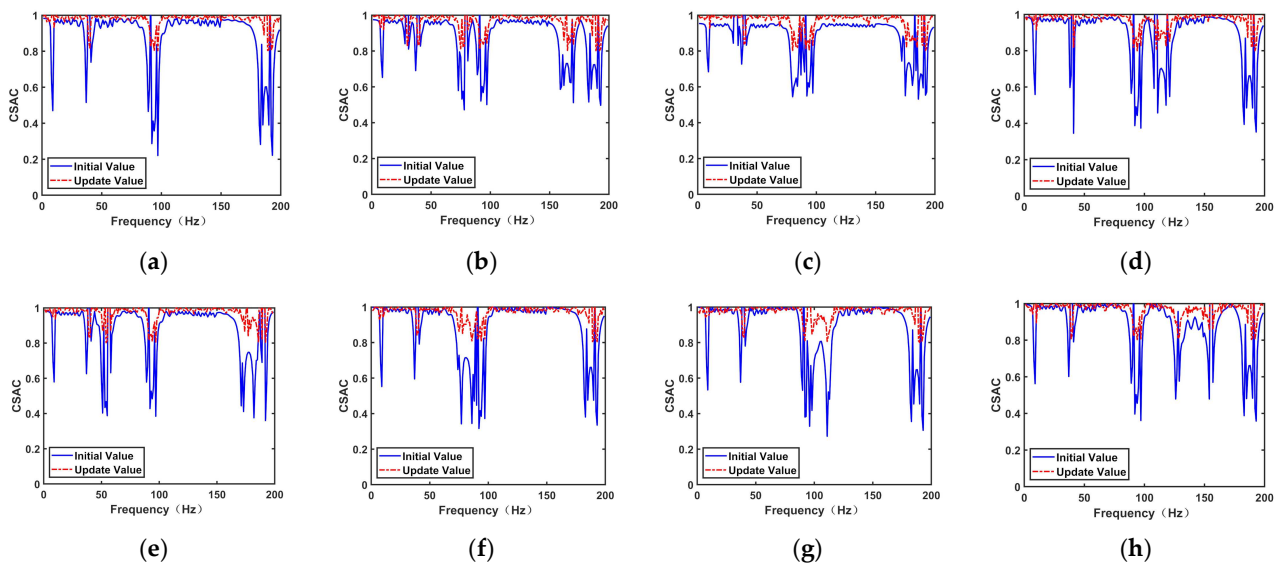


**Figure 10.** Comparison of CSF: (a–h) represent the comparison of CSF at sensor measuring points 1, 2, 3, 4, 5, 6, 7, 8.

#### 4.3. Validity of Motion Control

Based on the above analysis, a dynamic prediction model is formulated to consider clearance influence. Matlab/Simulink and Carsim are used to establish the sliding mode control model based on the clearance model (SMC-CM) for performance evaluation by introducing the dynamic prediction model into the sliding mode control system. To assess the feasibility of the SMC-CM, the sliding mode control (SMC) was compared to the SMC-CM at a speed of 72 km/h. Then, SMC-CM was compared with MPC and SMC to verify its superiority at 120 km/h.

As can be seen from the comparison results between SMC-CM and SMC at 72 km/h speed, both lateral position error and yaw velocity can be maintained within a tight range in Figure 11. Table 3 illustrates the lateral position error and yaw velocity peak pairs for different control methods. In comparison with SMC, the SMC-CM tracking error peak has

decreased by approximately 21.2%, and reliability has improved by approximately 12.7%. The results indicate that SMC-CM is a viable solution under low-speed conditions.

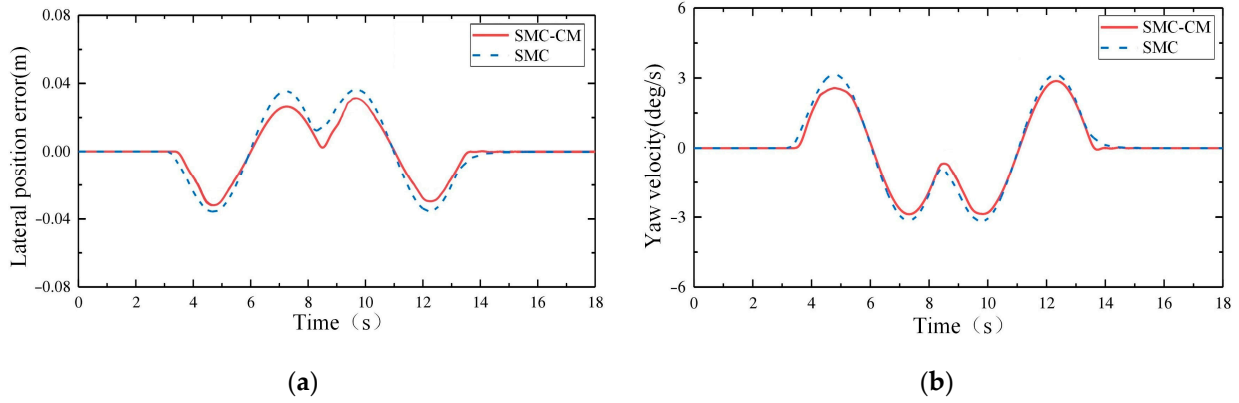


Figure 11. Error results at 72 km/h speed: (a) is lateral position error; (b) is yaw velocity error.

Table 3. Comparison of different control methods.

Parameter	SMC-CM	SMC
Lateral position error (m)	0.025	0.033
Yaw velocity (deg/s)	2.83	3.24

In order to determine the control effect of the proposed control method in medium and high-speed driving, MPC, SMC, and SMC-CM results were compared to verify the superiority of SMC-CM at high speed.

Figure 12 illustrates the results of the lateral position error and heading angle error. The maximum errors of the three controllable methods all occur near the maximum curvature. These errors are shown in Table 4. Compared with the MPC, the lateral position error peak and heading error peak of SMC-CM are reduced by 50% and 35.7%. In comparison with SMC, the lateral position error peak value and the heading error peak of SMC-CM are reduced by 14.3% and 15.6%. The accuracy of SMC-CM is superior to MPC and has superior improvement over SMC.

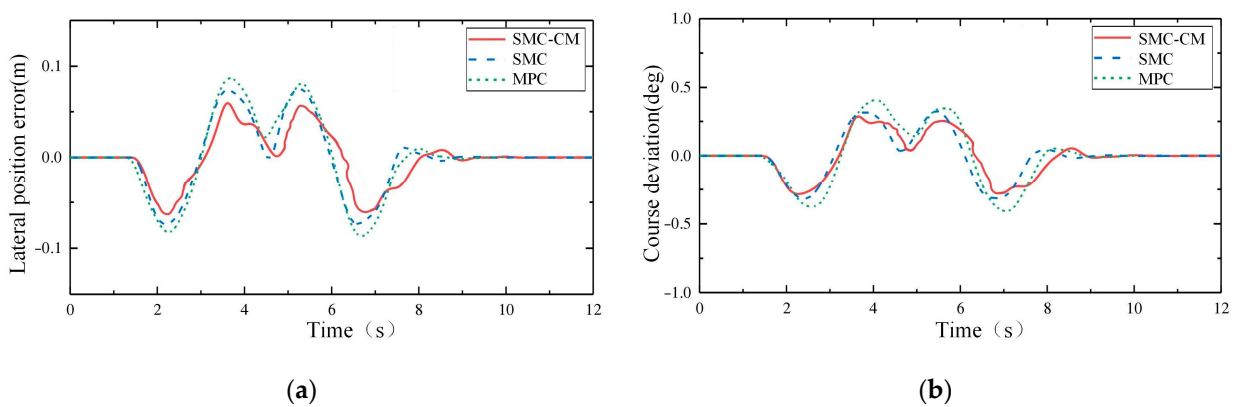
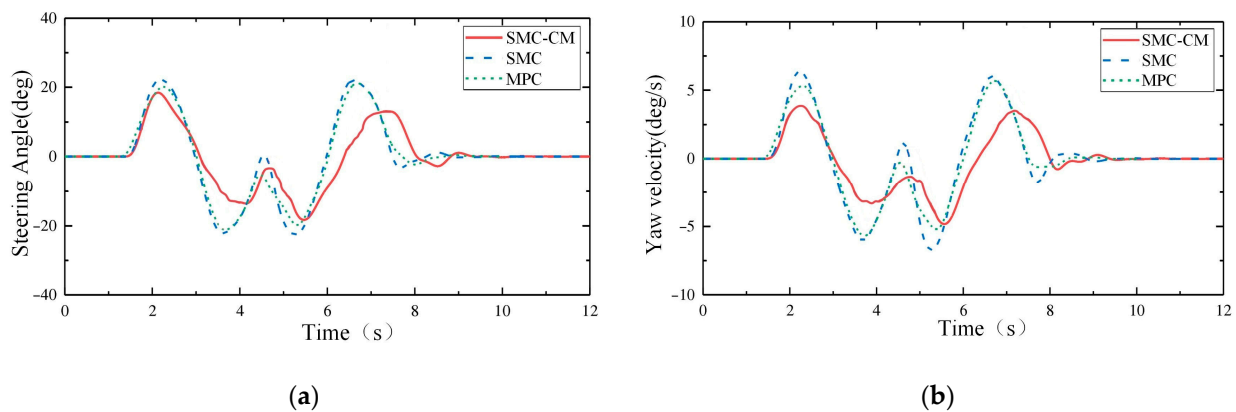


Figure 12. Error results at high speed: (a) is lateral position error; (b) is yaw velocity error.

**Table 4.** Error comparison of different control methods.

Parameter	SMC-CM	SMC	MPC
Lateral position error (m)	0.06	0.07	0.12
Yaw velocity (deg/s)	0.27	0.32	0.42

Figure 13 depicts a comparison of yaw velocity and lateral acceleration. Table 5 illustrates the peak reliability of MPC, SMC, and SMC-CM. In comparison with MPC, the SMC-CM has a 23.5% increase in peak yaw velocity and a 27.8% increase in peak lateral acceleration. The peaks are reduced by 3.7% and 18.8% compared to SMC. The results indicate that the lateral reliability of SMC-CM is superior to MPC.

**Figure 13.** Error results: (a) is lateral acceleration error; (b) is yaw velocity error.**Table 5.** Peak reliability comparison of different control methods.

Parameter	SMC-CM	SMC	MPC
Lateral acceleration (deg/s <sup>2</sup> )	−5.2	−5.4	−6.8
Yaw velocity (deg/s)	−2.6	−3.2	−3.6

In simulation experiments, SMC-CM further improved the vehicle tracking effect compared to SMC and MPC. The tracking effect is optimized further for variable speeds and curvatures. On a real device, the radial displacement sensor is arranged vertically on the transmission shaft bench to measure the radial vibration. In other words, the two measuring points are 90 degrees apart. Sensors for X and Y directions are located on either side of the vertical centerline and are positioned as close as possible to the shaft. In addition to a wide range of interference factors in the measurement process, noise reduction of vibration data is also a major concern. In order to adjust the driving state of the vehicle, a motion control system predicts the vibration law of the drive shaft using the analyzed data.

## 5. Conclusions

Vibration reduces the transmission shaft control accuracy and the response time resulting from the clearance. The intelligent shaft is abstracted to a cantilever beam with double clearance to forecast vibrations for error compensation by introducing time-varying parameters. The results show the following:

1. With the Hamilton principle and the assumed modal method, a dynamic model of the cantilever beam with double clearance is constructed. A clearance modeling method is proposed to describe clearance dynamics with time-varying parameters. A wavelet transform was used to identify the time-varying stiffness of clearance by estimating the natural frequency and damping ratio. The time-varying damping

of clearance was constructed using Rayleigh and complex damping. The clearance model accurately describes the dynamical clearance variation using time-varying damping and stiffness.

2. An experimental model was constructed to verify the proposed modeling method. Compared to the constant model, the maximum natural frequency error of the time-varying model was reduced from 5.38% to 1.29%. The maximum MAC also increased from 0.4173 to 0.8492. The MRE and RMSE of each measurement point decreased by 27.67% and 63.41%. The FRAC increased from 0.7971 to 0.9465. CSAC and CSF increased by 6.55% and 12.37%, which is over 90%, particularly near the natural frequency position. Therefore, the above results demonstrate the validity and accuracy of the modeling method.
3. The control method based on the clearance model was verified. At 72 km/h, compared with SMC, the tracking error peak of SMC-CM decreased by 21.2% and the reliability increased by 12.7%. Compared to MPC and MSC, the lateral position error peak of SMC-CM decreased by 50% and 14.3%, the heading error peak decreased by 35.7% and 15.6%, and the yaw velocity peak decreased by 23.5% and 3.7%. Peak lateral accelerations decreased by 27.8% and 18.8%. The effectiveness of the control method is verified.

This paper aims to examine the influence of mechanical transmission system errors on control system accuracy. In the future, tracking effects and handling reliability will be improved in extreme conditions. The influence of clearance factors in other vehicle mechanical systems on handling reliability and safety will also be considered, along with optimizing the control system.

**Supplementary Materials:** The following supporting information can be downloaded at: <https://www.mdpi.com/article/10.3390/su14116698/s1>, The data: The data of FRF.

**Author Contributions:** Writing—original draft, Y.Z.; Writing—review & editing, F.Z., W.W., F.M., D.Z. and H.W. All authors have read and agreed to the published version of the manuscript.

**Funding:** This research is supported by the State Department project of China (Grant No. JCKY20172 08A001, MKF20200022) and the National Science Fund of China (Grant No. 51805502). The authors gratefully acknowledge the facilities provided by the Industrial and Intelligent System Engineering Laboratory (IISEL) at the Beijing Institute of Technology.

**Data Availability Statement:** The data is in the Supplementary Materials.

**Conflicts of Interest:** The authors declare no conflict of interest.

## References

1. Wang, W.; Bengler, K.; Jiang, X. Green Intelligent Transportation Systems. In Proceedings of the 7th International Conference on Green Intelligent Transportation System and Safety, Nanjing, China, 1–4 July 2016; Wang, W., Bengler, K., Jiang, X., Eds.; Lecture Notes in Electrical Engineering. Springer: Singapore, 2018; Volume 419.
2. Fu, T.; Yao, C.; Long, M.; Gu, M.; Liu, Z. Overview of Longitudinal and Lateral Control for Intelligent Vehicle Path Tracking. In Proceedings of the Chinese Intelligent Automation Conference, Jiangsu, China, 20–22 September 2019.
3. Colbaugh, R. Adaptive Stabilization of Mobile Manipulators. *J. Robot. Syst.* **1998**, *15*, 511–523. [[CrossRef](#)]
4. Huang, L. Speed Control of Differentially Driven Wheeled Mobile Robots—Model-Based Adaptive Approach. *J. Robot. Syst.* **2005**, *22*, 323–332. [[CrossRef](#)]
5. Pu, S.T.; Li, S.W.; Fan, R.C.; Ter-Feng, W. Point Stabilization Control of a Car-like Mobil Robot in Hierarchical Skew Symmetry Chained Form. In Proceedings of the IEEE International Conference on Networking, Sensing and Control, Taipei, Taiwan, 21–23 March 2004; IEEE: Taipei, Taiwan, 2004; Volume 2, pp. 1346–1351.
6. Fierro, R.; Lewis, F.L. Control of a Nonholonomic Mobile Robot: Backstepping Kinematics into Dynamics. *J. Robot. Syst.* **1997**, *14*, 149–163. [[CrossRef](#)]
7. Dixon, W.E.; Dawson, D.M.; Zhang, F.; Zengeroglu, E. Global Exponential Tracking Control of a Mobile Robot System via a PE Condition. *IEEE Trans. Syst. Man Cybern. Part B* **2000**, *30*, 129–142. [[CrossRef](#)]
8. Tayebi, A.; Rachid, A. Adaptive Controller for Non-Holonomic Mobile Robots with Matched Uncertainties. *Adv. Robot.* **2000**, *14*, 105–118. [[CrossRef](#)]

9. Lihan, S.; Jie, M.; Baoqing, Y. Fuzzy PID Design of Vehicle Attitude Control Systems. In Proceedings of the 2020 Chinese Control and Decision Conference (CCDC), Hefei, China, 22–24 August 2020; pp. 1826–1830.
10. Majid, M.; Arshad, M. A Fuzzy Self-Adaptive PID Tracking Control of Autonomous Surface Vehicle. In Proceedings of the 2015 IEEE International Conference on Control System, Computing and Engineering (ICCSCE), Batu Ferringhi, Penang, Malaysia, 27–29 November 2015; pp. 458–463.
11. Shuguang, W.; Xiaojun, M.; Qinghan, Z.; Chunguang, L. Adaptive Sliding Mode Wheel Slip Control of Electric Vehicles Based on Feedback Linearization. *Fire Control Command Control* **2016**, *41*, 23–27.
12. Temiz, O.; Cakmakci, M.; Yildiz, Y. A Fault Tolerant Vehicle Stability Control Using Adaptive Control Allocation. In Proceedings of the Dynamic Systems and Control Conference, Atlanta, GA, USA, 30 September–3 October 2018; Volume 51890, pp. 1–9.
13. Lucibello, P.; Oriolo, G. Robust Stabilization via Iterative State Steering with an Application to Chained-Form Systems. *Automatica* **2001**, *37*, 71–79. [[CrossRef](#)]
14. Yongoug, C.; Chongkug, P.; Harashima, F. A Position Control Differential Drive Wheeled Mobile Robot. *IEEE Trans. Ind. Electron.* **2001**, *48*, 853–863. [[CrossRef](#)]
15. Hamel, T.; Meizel, D. On Robustness and Precision of Mobile Robots Missions. *Automatica* **2001**, *37*, 437–444. [[CrossRef](#)]
16. Lee, T.C. Practical Stabilization for Nonholonomic Chained Systems with Fast Convergence, Pole-Placement and Robustness. In Proceedings of the 2002 IEEE International Conference on Robotics and Automation, Washington, DC, USA, 11–15 May 2002; Volume 4, pp. 3534–3539.
17. Ying, M.J. Robust Control with Decoupling Performance for Steering and Traction of 4WS Vehicles under Velocity-Varying Motion. *IEEE Trans. Contr. Syst. Technol.* **2000**, *8*, 554–569.
18. Xu, X.; Mi, J.; Wen, C.Y.; Wang, F.; Ma, S.D.; Tao, T. Robust  $H_{\infty}$  Optimal Control for the Lateral Stability of Semitrailer Trucks. *Mod. Manuf. Eng.* **2019**, *45*, 1283–1293.
19. Li, P.; Li, P.; Zhao, J.; Zhang, B. Robust Gain-Scheduling Static Output-Feedback  $H_{\infty}$  Control of Vehicle Lateral Stability with Heuristic Approach. *Inf. Sci.* **2021**, *546*, 220–233. [[CrossRef](#)]
20. Chen, T.; Chen, D. Lateral Control of Intelligent Vehicle Based on Neural Networks Sliding Mode. *Transducer Microsyst. Technol.* **2017**, *36*, 63–67.
21. Chang, Z.; Hao, L.; Yan, Q.; Ye, T. Research on Manipulator Tracking Control Algorithm Based on RBF Neural Network. *J. Phys. Conf. Ser.* **2021**, *1802*, 032072. [[CrossRef](#)]
22. Jia, L.; Zhu, Z. Improved Fractional-Order Integral Sliding Mode Control for AUV Based on RBF Neural Network. In Proceedings of the 2019 Chinese Automation Congress (CAC), Hangzhou, China, 22–24 November 2019; pp. 4809–4814.
23. Henaff, P.; Chocron, O. Adaptive Learning Control in Evolutionary Design of Mobile Robots. In Proceedings of the IEEE International Conference on Systems, Man and Cybernetics, Yasmine Hammamet, Tunisia, 6–9 October 2022; Volume 3, p. 5.
24. Kim, S.; Kim, T.I.; Jang, K.S.; Jung, S.; Kim, S.S. Control Experiment of a Wheeled Drive Mobile Pendulum Using Neural Network. In Proceedings of the 30th Annual Conference of IEEE Industrial Electronics Society, Busan, Korea, 2–6 November 2004; Volume 3, pp. 2234–2239.
25. Rusu, P.; Petriu, E.M.; Whalen, T.E.; Cornell, A.; Spoelder, H.J. Behavior-Based Neuro-Fuzzy Controller for Mobile Robot Navigation. *IEEE Trans. Instrum. Meas.* **2003**, *52*, 1335–1340. [[CrossRef](#)]
26. Wang, Z.; Ge, S.; Lee, T. Adaptive Neural Network Control of a Wheeled Mobile Robot Violating the Pure Nonholonomic Constraint. In Proceedings of the 2004 43rd IEEE Conference on Decision and Control, Atlantis, Paradise Island, Bahamas, 14–17 December 2004; Volume 5, pp. 5198–5203.
27. Fierro, R.; Lewis, F.L. Control of a Nonholonomic Mobile Robot Using Neural Networks. *IEEE Trans. Neural Netw.* **1998**, *9*, 589–600. [[CrossRef](#)]
28. Choomuang, R.; Afzulpurkar, N. Hybrid Kalman Filter/Fuzzy Logic Based Position Control of Autonomous Mobile Robot. *Int. J. Adv. Robot. Syst.* **2005**, *2*, 20. [[CrossRef](#)]
29. Maalouf, E.; Saad, M.; Saliyah, H. A Higher Level Path Tracking Controller for a Four-Wheel Differentially Steered Mobile Robot. *Robot. Auton. Syst.* **2006**, *54*, 23–33. [[CrossRef](#)]
30. Butcher, M.; Karimi, A.; Longchamp, R. A Statistical Analysis of Certain Iterative Learning Control Algorithms. *Int. J. Control* **2008**, *81*, 156–166. [[CrossRef](#)]
31. Utkin, V.; Poznyak, A.; Orlov, Y.; Polyakov, A. Conventional and High Order Sliding Mode Control. *J. Frankl. Inst.* **2020**, *357*, 10244–10261. [[CrossRef](#)]
32. Tian, Q.; Xiao, Q.; Sun, Y.; Hu, H.; Liu, H.; Flores, P. Coupling Dynamics of a Geared Multibody System Supported by ElastoHydroDynamic Lubricated Cylindrical Joints. *Multibody Syst. Dyn.* **2015**, *33*, 259–284. [[CrossRef](#)]
33. Liu, J.; Li, B. Theoretical and Experimental Identification of Clearance Nonlinearities for a Continuum Structure. *J. Comput. Nonlinear Dyn.* **2016**, *11*, 041019. [[CrossRef](#)]
34. Yang, G.; Yang, J.; Qiang, C.; Ge, J.; Chen, Q. Natural Frequencies of a Cantilever Beam and Block System with Clearance While Block Staying on given Position. *J. Vib. Control* **2013**, *19*, 262–275. [[CrossRef](#)]
35. Bai, Z.F.; Zhao, Y. Dynamic Behaviour Analysis of Planar Mechanical Systems with Clearance in Revolute Joints Using a New Hybrid Contact Force Model. *Int. J. Mech. Sci.* **2012**, *54*, 190–205. [[CrossRef](#)]
36. Khatiwada, S.; Chouh, N.; Butterworth, J.W. A Generic Structural Pounding Model Using Numerically Exact Displacement Proportional Damping. *Eng. Struct.* **2014**, *62–63*, 33–41. [[CrossRef](#)]



37. Marques, F.; Isaac, F.; Dourado, N.; Flores, P. An Enhanced Formulation to Model Spatial Revolute Joints with Radial and Axial Clearances. *Mech. Mach. Theory* **2017**, *116*, 123–144. [[CrossRef](#)]
38. Liu, J.; Li, B.; Jin, W.; Han, L.; Quan, S. Experiments on Clearance Identification in Cantilever Beams Reduced from Artillery Mechanism. *J. Mech. Eng. Sci.* **2017**, *231*, 1010–1032. [[CrossRef](#)]
39. Mayergoyz, I.D. *Mathematical Models of Hysteresis and Their Applications*; Academic Press: New York, NY, USA, 2003.
40. Goldsmith, W.; Frasier, J.T. Impact: The Theory and Physical Behavior of Colliding Solids. *J. Appl. Mech.* **1961**, *28*, 639. [[CrossRef](#)]
41. Xu, C.; Wang, C.; Gao, J. Modal Identification of Linear Time-Varying Systems Using Continuous Wavelet Transform. *J. Harbin Inst. Technol.* **2015**, *22*, 30–36.
42. Hu, G. *Modern Signal Processing Course*; Tsinghua University Press: Beijing, China, 2004.
43. Rayleigh, J.; Lindsay, R.B. *The Theory of Sound*; Dover Publications: New York, NY, USA, 1945; Volume 2.
44. Myklestad, N.O. The Concept of Complex Damping. *J. Appl. Mech.* **1952**, *19*, 284–286. [[CrossRef](#)]
45. Dong, X.Y.; Peng, Z.R.; Yin, H.; Dong, H.T. Distance Coefficient-Fisher Information Criterion for Optimal Sensor Placement. *CAAI Trans. Intell. Syst.* **2017**, *12*, 32–37.
46. Wen, H.B.; Wang, G.Z. Updating Finite Element Model of Cabin with Floating Raft through Sensitivity Analysis of FEF Correlation Coefficient. *J. Jiangsu Univ. Sci. Technol.* **2005**, *19*, 75–78.